University of Glasgow

DEPARTMENT OF

AEROSPACE ENGINEERING

An investigation of three-dimensional dynamic stall

by

R.A.McD. Galbraith, F.N. Coton,
and D.Jiang

An investigation of three-dimensional dynamic stall

by

R.A.McD. Galbraith, F.N. Coton,
and D.Jiang

Final contractor report for SERC/EPSRC contract number GR/H48330

December 1995

G.U. Aero. Report 9542

AN INVESTIGATION OF THREE-DIMENSIONAL DYNAMIC STALL

R.A.McD Galbraith, F.N. Coton, D.Jiang
Department of Aerospace Engineering
University of Glasgow
GLASGOW
G12 8QQ

Final contractor report for SERC/EPSRC contract number GR/H48330

ABSTRACT

The following report summarises a three year research programme in the Department of Aerospace Engineering, University of Glasgow to collect unsteady pressure data on the dynamic stalling characteristics of finite wing planforms. The original motivation for the work lay in the pressing need for a greater understanding of the strongly three-dimensional effects in the tip region of helicopter rotors. In this study, a new data collection system capable of sampling 200 parallel channels at up to 50kHz per channel has been developed. Additionally, a new support structure, actuation mechanism and hydraulic supply system was established for the test programme. Together, these new systems were used to conduct tests on two wing planforms; a straight rectangular wing and a rectangular wing with 60° swept tips. A final model, of a 60° delta wing, is currently being instrumented and will be tested in January 1996. Although the emphasis of the original proposal was on data collection, analysis of preliminary results has been presented at the European Rotorcraft Forum and a related paper is currently being reviewed for publication in a journal. The pressure data collected are of extremely high quality and are the most detailed of their type currently available. In addition, these have been supplement by extensive flow visualisation tests using a state of the art image capturing system. The resulting combined data set has highlighted many of the salient features of three-dimensional dynamic stall and, as originally intended, should provide a basis for future research in this area.

OBJECTIVES

The primary objective of the work was provide high quality data to permit the assessment of fundamental phenomena associated with the dynamic stalling of finite wings.

METHODOLOGY

The Department of Aerospace Engineering at Glasgow University has an established track record in the dynamic stall testing of aerofoil sections. The methodology, developed over several years, was extended in this project to the study of the dynamic stalling of finite wings. In particular, high frequency acquisition of surface pressure data at a large number of surface locations formed the backbone of the study. This was supplemented by smoke flow visualisation studies in a purpose built facility and utilising a 25 frames/second full screen digital video capturing system. Data reduction and presentation was performed on two dedicated computer platforms.

VARIATION FROM THE ORIGINAL PROPOSAL

It was originally proposed that three wing planforms should be tested during the study. Of these, two have been tested and the third is being instrumented. The delay in the testing programme has resulted from a combination of circumstance, mainly outwith the control of the investigators. Nevertheless, the programme will be completed and the data supplied to the collaborating bodies as originally proposed, albeit slightly late. In addition, as a result of consultations with DERA and Westland Helicopters, the third model has been manufactured with a removable nose section to allow a study of the effect of this region on the formation of vortices on the delta wing. Thus, on completion of the proposed programme, tests will be conducted on a variant of the third model, a round nosed delta wing, to investigate this effect. These additional tests will be conducted at the expense of Glasgow University.

Another change to the proposed programme relates to the smoke flow visualisation work. Originally it was intended that tests would only be conducted to aid in the location of pressure transducers. In fact, a much more extensive programme of flow visualisation was conducted to examine specific flow phenomena associated with the stalling process on all three planforms. Additional funding for this aspect of the work was attracted through a vacation scholarship awarded by the Nuffield Foundation (Moir & Coton (1995))

DETAILED DESCRIPTION OF WORK PROGRAMME

Wind Tunnel and Test Rig

The tests were carried out in the University of Glasgow's 'Handley Page' wind tunnel which is a low-speed closed-return type. The wing model was located horizontally in its 2.13 × 1.61 metre octagonal working section and supported on three struts, as shown in Fig. 1. These were, in turn, connected to the main support structure and actuation mechanism which was situated below the tunnel. Movement of the model was produced by

displacement of the two rear struts and the model was pivoted about the quarter chord position on a tool steel shaft connected to the front support via two self aligning bearings. The actuation force was produced using a Parker 2H Series linear hydraulic actuator and crank mechanism which allowed a variation of angle of attack from -26^{o} to 45^{o}. This system comprised the 2H series hydraulic cylinder, a bridge manifold, a high response proportional directional control valve with a E200-595 PID analogue closed loop controller and could deliver a maximum thrust of 17KN during extension and 6.53 KN during retraction at a piston speed of 1.1m/s. An angular displacement transducer mounted on the crank was used to provide a feedback signal and for recording the real time angle of attack.

The required motion profile was provided by an AMSTRAD 1512 microcomputer equipped with an ANALOG DEVICES RT1815 multi-function input/output board. The required output function was digitised into equal time steps in 2's complement code and the frequency was controlled using interrupts on the AMSTRAD microcomputer. The computer programme was written in TURBO PASCAL.

Test Models

The first test model was a straight wing with a NACA 0015 cross-section. The wing, which is shown in Fig. 2., had simple solids of revolution at its tips. The AR of this model was chosen as 3.0 to maximise the chord Reynolds number whilst avoiding strong three-dimensionality at the mid-span in steady flow and minimising blockage effects. The final overall dimensions were 126cm × 42cm which resulted in a variation of model blockage from a minimum of 2.6% to a maximum of 11.35% (not including the faring of struts) and a model span to tunnel width ratio of 0.592. According to previous studies of the blockage effect for 2-D dynamic stall testing (Green & Galbraith (1994)) these dimensions were considered acceptable. The model was constructed with an aluminium framework of ribs and stringers and an outer epoxy glass fibre skin. Figure 2 illustrates this construction.

The second test model was a rectangular wing with 60^{o} swept tips. This model was constructed in the same manner as the first model and had the same chord length and trailing edge dimensions. The wing tips progressed from solids of revolution at the leading edge to sharp edges after the mid-chord. The overall geometry of this model was chosen in tri-partite discussions with DERA and Westland Helicopters.

The final model was a sharp edged 60^{o} delta wing of length 80cm from base to apex. The main body of this model was machined from solid aluminium and the top surface from an aluminium plate. As mentioned previously, the model has a detachable nose section to allow the effects of other nose profiles to be assessed in the future.

Instrumentation and Data Logging

Altogether, 192 pressure transducers were placed within each model predominantly to the starboard side. On the first model there were six chordal distributions at various spanwise locations, each of which had 30 transducers. In the region of the tip, additional transducers were placed between the above mentioned sections to provide a better assessment of the tip vortex movement and structure. In order to check on the overall symmetry of the flow, two transducers were placed on the left side of the wing in corresponding positions to their counterparts on the starboard side. It is worthy of note that the signals recorded on these transducers indicated that in most cases little asymmetry existed (Galbraith et al. (1995)). Additionally three accelerometers were embedded in the wing, two of which were at the rear tip locations and a final one mounted centrally. On the delta wing transducers were aligned in rows parallel to the base. The intermediate swept profile was instrumented using a combination of the strategies used for the other two wings.

All pressure transducers were of kulite differential type CJQH-187 with one side of the pressure diaphragm open to the ambient pressure outside the wind-tunnel via tubing. The signals from all of the transducers were taken to a specially designed signal conditioning unit of modular construction with each module containing its own control board. On instruction from the computer, the control board automatically removed all offsets to below the A-D converter resolution and adjusted all gains as necessary. In fact, during a test the computer sampled the maximum and minimum of each transducer output and adjusted the gains accordingly to improve the data acquisition resolution. The data acquisition was carried out by a PC microcomputer, configured with a 486 processor and interfaced with proprietary Backer BE256 modules which provided the necessary analogue to digital conversion. The software used for data acquisition was TEAM 256. At present, the system has 200 channels, each of which is capable of sampling to a maximum rate of 50KHz, giving an overall sampling rate of 10MHz.

The reference dynamic pressure in the wind tunnel working section was determined by measuring the difference between the static pressure in the working section, upstream of the leading edge of the model, and the static pressure in the settling chamber. The pressure tappings were connected to a FURNESS FC012 micromanometer, which provided an analogue signal suitable for the data acquisition unit.

Test series and procedure

Four particular types of tests were considered in this study. These were static tests, ramp up tests, ramp down tests and sinusoidal tests. In all cases, the model was rotated about its quarter-chord axis to achieve the desired motion type. In the static tests, the wing was positioned at the incidence at which the first set of data was to be recorded. Usually, this was approximately -5^{o}. The model's angle of attack was then increased in steps of 1^{o} up to 42^{o} allowing an appropriate settling time at each angle.

During a ramp test, the wing was rotated over a pre-set arc at a constant pitch-rate. For the lower pitch rates, excellent ramp functions were obtained but, at the higher values, the starting and stopping sequences induced non-linearities. The ramp motion was repeated several times at each pitch rate and data from 4 cycles of motion were recorded.

In the oscillatory tests, the model was pitched about a mean angle in such a manner that its angle of attack varied sinusoidally with time. The mean angle, amplitude and frequency were controlled by the AMSTRAD function generator and 8 cycles of motion were recorded. The test series for the first model is shown as an example in Table 1.

Data storage , reduction and presentation

All the binary data collected by the acquisition system were initially stored on the PC prior to being downloaded to DAT tape through a HP35470A DAT drive. The raw data on DAT tape was then read and reduced on a SUN SPARC 10 workstation using a dedicated code written in C language. Both the raw data and the reduced data were then archived onto DAT tape. The reduced data were stored in ASCII files identified by a run number. These files were composed of a run information block and the reduced data measured from 200 transducers.

Previous experience has shown that there exist minor random differences in data from cycle to cycle for dynamic tests and that the salient features are highlighted by the averaging process. The main data presented in this report are the average of those from a number of consecutive cycles. For ramp tests, the reduced data for each transducer are the average of 4 cycles of 8000 samples. For sinusoidal tests an average of 8 cycles of 4000 samples was used. A FORTRAN program was used to produce the integrated force and moment coefficients presented in this report. All graphical presentations were made using the PV WAVE software suite.

Test Data

For every run, a fixed number of pages of plots were used to present the main features of the measured data. In the case of the first model, this amounted to 16 pages per test. It should be noted that of the 8000 measurements taken at each transducer location during an individual test, only one in twenty, forty or eighty of the points were plotted on the graphs presented in standard data reports (Jiang et al. (1995a,b,c,d,e,f,g,h) and Jiang et al. (1995i,j,k,l,m,n,o,p)). Use of higher resolution, whilst beneficial when examining a specific feature of short-duration, is limited by line thickness when surface plotting over the entire incidence range.

Smoke Flow Visualisation Tests

Tests were conducted in the University of Glasgow 0.91m x 0.91m flow visualisation wind tunnel. The pitching motion of the model was generated by use of a stepper motor/lead screw system. The stepper motor was programmed using LABVIEW running on a Macintosh LCIII computer with a data acquisition board installed. Smoke was produced by vaporising Ondina oil in a Taylor Scientific smoke generator and was introduced to the flow either through small holes in the model surface or from a smoke-rake positioned upstream of the model. Images were recorded using a camcorder and then transferred to digital form via the Macintosh based Videovision Studio frame grabbing system at 25 frames per second.

SAMPLE DATA AND PRELIMINARY ANALYSIS

In this section, sample data from the first model is presented and a brief analysis of these results is given. The particular case is that of a ramp-up between -5 and +38 degrees at a linear pitch rate of 411 degrees per second resulting in a reduced pitch rate of 0.027. Whilst being a particularly interesting case, it also serves to illustrate the quality of the data and the range of information available from the study.

Figure 3 presents the variations of the local normal force coefficients at the six instrumented span locations. In each case, the measured static characteristic at the particular spanwise station is provided for reference. A feature common to all of the plots is the incidence reversal after the end of the ramp motion. This was caused by limitations of the hydraulic system and was a control response to an initial overshoot at the end of the ramp phase. Other studies have shown, however, that the dominant features of the unsteady flowfield appear relatively insensitive to this type of behaviour. Nevertheless, it is pertinent to note that only the very fast ramp cases, where the hydraulic actuation system was operating at its design limit, were affected in this way.

The force coefficients presented in Fig. 3. were obtained by integration of chordwise pressure distributions at the relevant spanwise locations. It has been shown, for ramp motions, that the most significant features of these pressure distributions are manifest on the upper surface. Figure 4 illustrates the variation of the upper-surface chordwise pressure distribution, with the temporal change in incidence, at two of the spanwise positions, shown above. At 57.14% of span, the pressure distribution is characterised by the classical growth of leading edge suction as the incidence increases. Additionally, there is no obvious sign of trailing edge separation, even above 20 degrees. At approximately 30 degrees there is incipient leading edge suction peak collapse. At the same time, a suction bulge develops just behind the leading edge and then moves rearwards with time. During its progression towards the trailing edge, this suction bulge loses definition but can be clearly observed leaving the trailing edge after the end of the ramp. After this, a second area of suction appears near the quarter chord and moves towards the trailing edge, losing definition as it goes. It is worthy of note that many of the features observed here are akin to those of nominally two-dimensional flows (Galbraith et al. (1995)).

In the 97.2% of span case, the build up of suction at the leading edge is much less significant than the previous case. It is, however, accompanied by a build up of suction at the trailing edge which starts at very low positive incidence. As the ramp progresses, this area of suction increases in strength and occupies more of the chord until finally it disappears as the suction peak collapses. Subsequently, there is a slight recovery of suction at the leading edge before a secondary collapse.

In steady flow, the spanwise loading distribution on a finite wing is dominated by the downwash from the wing tip vortices which becomes more significant nearer the wing tips and acts to reduce the effective incidence there. This is clearly illustrated in Fig.3. where the gradient of the steady flow Cn curves is lower on outboard sections than those close to the mid span. If this effect was reproduced during ramp-up motion, an inevitable consequence would be a spanwise variation of effective pitch rate on the wing. Evidence of this can be observed in Fig.3. where the Cn curves for the ramp-up case closely follow those measured for steady flow at low incidence. Given that the ramp motion is nominally linear, this result indicates higher effective pitch rates at the mid span than near the wing tips. Since, for the two-dimensional case, it is generally accepted that the severity of the dynamic stall process is closely related to pitch rate, the finite wing should produce a dynamic stall vortex which is non-uniformly distributed along the span.

As indicated above, many of the basic features of the Cn curves measured near the mid-span in the present study are similar to those of the two-dimensional case. At the 57.14% of span location, it is noticeable that the increased growth in Cn, caused by the dynamic stall vortex, is short lived. This is consistent with the corresponding upper surface pressure distribution variation shown in Fig. 4. where, although the suction bulge of the vortex appears near the leading edge, it is not as great as would be expected in the two-dimensional case. There is also very little evidence of vortex build-up with convection occurring almost immediately. At this point, the leading edge suction peak collapses and Cn stall occurs. With the subsequent movement of the dynamic stall vortex, it becomes less distinct and less influential on the post stall Cn. One possible explanation for this behaviour is forthcoming from the work of Horner et al. (1990) who conducted flow visualisation experiments on an oscillating flat plate. Their work, although conducted at much lower Reynolds numbers than the present study, noted that a dynamic stall vortex did indeed form along most of the span but that the portion of the vortex at the mid-span lifted off the surface during its downstream convection. This observation was confirmed by a recent smoke flow visualisation study conducted by Moir & Coton (1995) on a wing with the same aspect ratio as the instrumented wing but, again, at a lower Reynolds number. In those tests it was observed that, although the initial formation of the dynamic stall vortex was almost uniform along the span, its subsequent development was highly three dimensional (Fig. 5). If this behaviour were repeated in the present case, the influence of the dynamic stall vortex on the measured pressure distribution at the mid-span would be expected to diminish as it lifted away from the surface. Initial convection of the vortex may also be initiated earlier as the vortex becomes more exposed to the influence of the freestream.

Figure 5, however, also shows that, away from the mid-span, the dynamic stall vortex curves down towards the surface at around 75% of span and is almost imperceptible further outboard. In fact, other views of this same flow structure indicate that the orientation of the dynamic stall vortex becomes almost perpendicular to the surface between 65% and 80% of span, depending on the downstream progression of the vortex system. Despite this, however, the vortex curves dramatically in the vicinity of the surface and retains connectivity with the wing-tip leading-edge through the weakened remainder of the dynamic stall vortex. Once this system reaches the mid-chord, it begins to interact with the collection of vorticity in the separated shear layer aft of the trailing edge separation line. Through this, the system achieves connectivity with the tip vortex system. This is clearly illustrated in the contour plot of surface pressures presented in Fig. 6 when the wing has just reached the end of the ramp arc. In the figure, which is generated by reflection of data from the instrumented side of the blade, the locations where the strong segments of the dynamic stall vortex arch down to the wing surface appear as well defined peaks of low pressure. From these, connectivity paths of low pressure extend to the leading and trailing edges at the wing tips. A low pressure area, corresponding to the effect of the elevated dynamic stall vortex, is

also evident at the mid-span. As the main segment of the dynamic stall vortex convects further aft, the connectivity with the leading edge diminishes and the two low pressure peaks are drawn slightly outboard before convecting off the trailing edge. This is, consistent with the Cn curve at 80% of span in which the change of gradient associated with the formation of the dynamic stall vortex and the magnitude of the peak Cn are less than would be expected in the nominally two-dimensional case but stall occurs much later.

At most of the span locations presented in Fig. 3, the Cn values measured during the early stages of the ramp motion exceed those obtained in the static test. Conversely, in previous two-dimensional tests, the dynamic coefficients were found to lag the steady values. The precise reason for this inconsistency is unclear but must, inevitably, be a consequence of the spanwise loading distribution on the wing during the pitching motion. From the discussion above, this implies that some aspect of the behaviour of the tip vortices, such as an increase in strength or a lateral inwards movement, may provide the required explanation. A more tangible effect of the tip vortices can be observed in the pressure distribution plot at 97.2% span presented in Fig. 4. Here, a substantial increase in suction is witnessed near the wing tips in the vicinity of the trailing edge. This suction is generated by the proximity of the tip vortex and, as the incidence increases, it becomes stronger and influences more of the trailing-edge corner of the wing. Finally, the collapse of leading edge suction and the associated reduction in circulation, rapidly diminishes the tip vortex strength.

These observations serve to highlight some of the salient features of the measured data from the first model. A more detailed discussion of these and other points can be found in Galbraith et al. (1995) and Galbraith et al. (1996).

CONCLUSIONS

During the present study, unsteady surface pressure data have been collected on two wing planforms. A third planform, a delta wing, will be tested in the near future. To achieve this, it has been necessary to design and built an actuation system, a 200 channel data collection system capable of 50kHz per channel, a model support system and three different wind tunnel models. This was a substantial undertaking which has resulted in high quality data being obtained.

Preliminary analyses have also been conducted on the data and the initial findings have been published. This aspect of the work is currently the subject of a follow-on proposal to the EPSRC.

REFERENCES

Galbraith RAMcD; Coton FN; Jiang D; Gilmour R (1995) Preliminary results from a three-dimensional dynamic stall experiment of a finite wing. 21st European Rotorcraft Forum, Russia

Galbraith RAMcD; Coton FN; Jiang D; Gilmour R (1996) An examination of dynamic stall on a pitching wing using high resolution pressure data. Submitted to the Journal of Experiments in Fluids

Green RB; Galbraith RAMcD (1994) A demonstration of the effect of the testing environment on unsteady aerodynamical experiments. Aero. Journal 98. pp83-90

Horner MB; Addington GA; Young III JW; Luttges MW (1990) Controlled Three-Dimensionality in Unsteady Separation Flows about a Sinusoidally Oscillating Flat Plate. AIAA- 90-0689

Jiang D; Coton FN; Galbraith RAMcD; Gilmour R (1995a,b,c,d,e,f,g,h) Collected data for tests on a NACA 0015 section rectangular wing (aspect ratio 3). Vols 1 - 8 GU Aero. Repts 9515 - 9522

Jiang D; Coton FN; Galbraith RAMcD; Gilmour R (1995i,j,k,l,m,n,o,p) Collected data for tests on a NACA 0015 section rectangular wing with 60° swept tips. Vols 1 - 8 GU Aero. Repts 9527 - 9534

Moir S; Coton FN (1995) An examination of the dynamic stalling of two wing planforms. G.U. Aero. Report 9526

Motion Type	Test Specifications				
Static	Reynolds No.	α Range (°)			No. of Tests
	1.0 x 10^6	-5 ~ 42			2
	1.5 x 10^6	-5 ~ 42			2
Ramp Up	Reynolds. No.	Starting α (°)	Ramp Arc (°)	Reduced Pitch Rate	No. of Tests
	1.5 x 10^6	-5	44	0.000091 ~ 0.029	60
	1.5 x 10^6	-5	20 ~ 40	0.02	5
Ramp Down	Reynolds No.	Starting α (°)	Ramp Arc(°)	Reduced Pitch Rate	No. of Tests
	1.5 x 10^6	39	44	-0.000097 ~ -0.029	38
	1.5 x 10^6	15 ~ 35	20 ~ 40	0.018	5
Sinusoidal	Reynolds No.	Mean α (°)	Amplitude (°)	Reduced Frequency	No. of Tests
	1.5 x 10^6	5 ~ 25	10	0.0092 ~0.17	38

Table 1. Model 1 test series

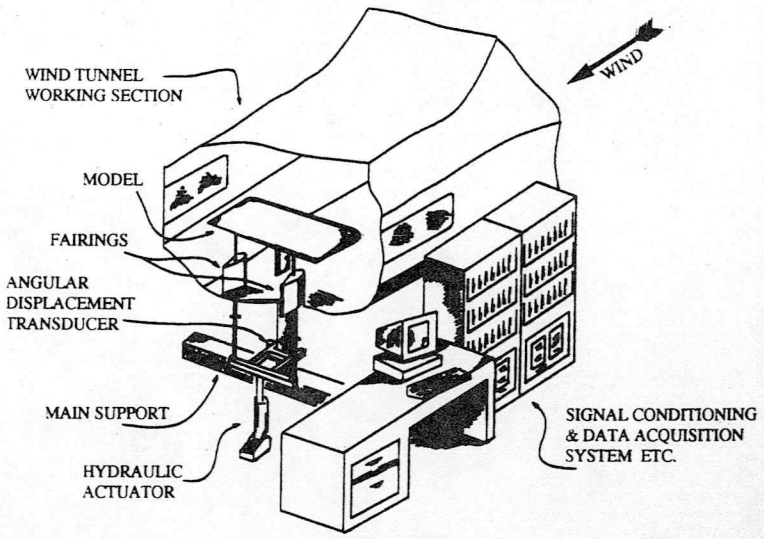

Fig. 1. Test set-up

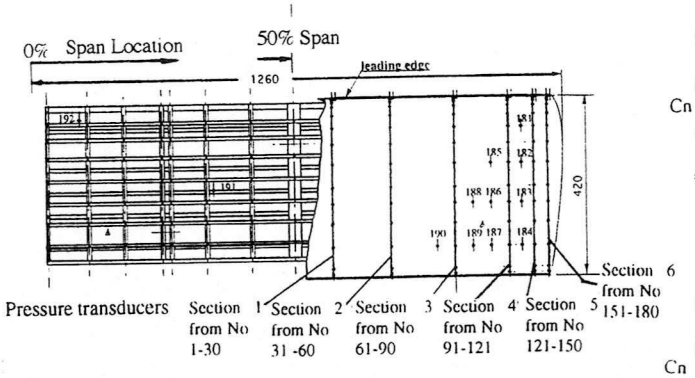

Fig. 2. Model 1 construction

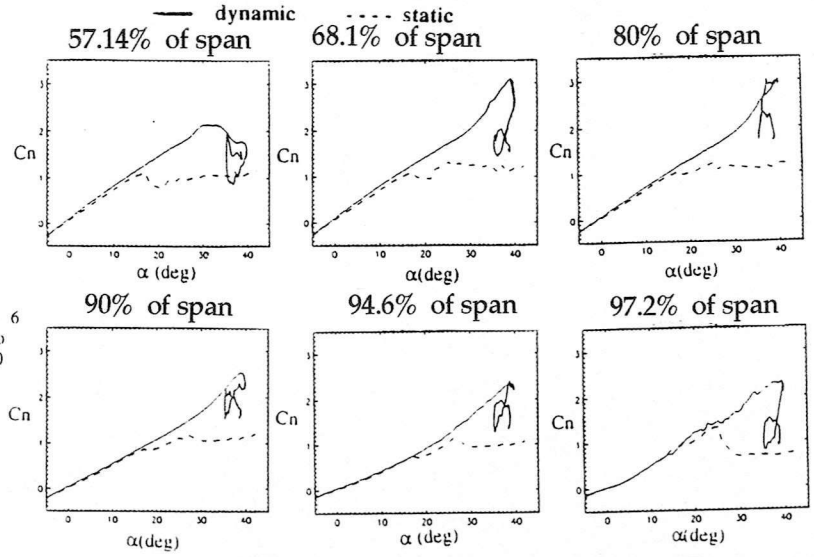

Fig. 3. Local Cn against α at six spanwise locations (Re = 1.5 x10^6, reduced pitch rate = 0.0272)

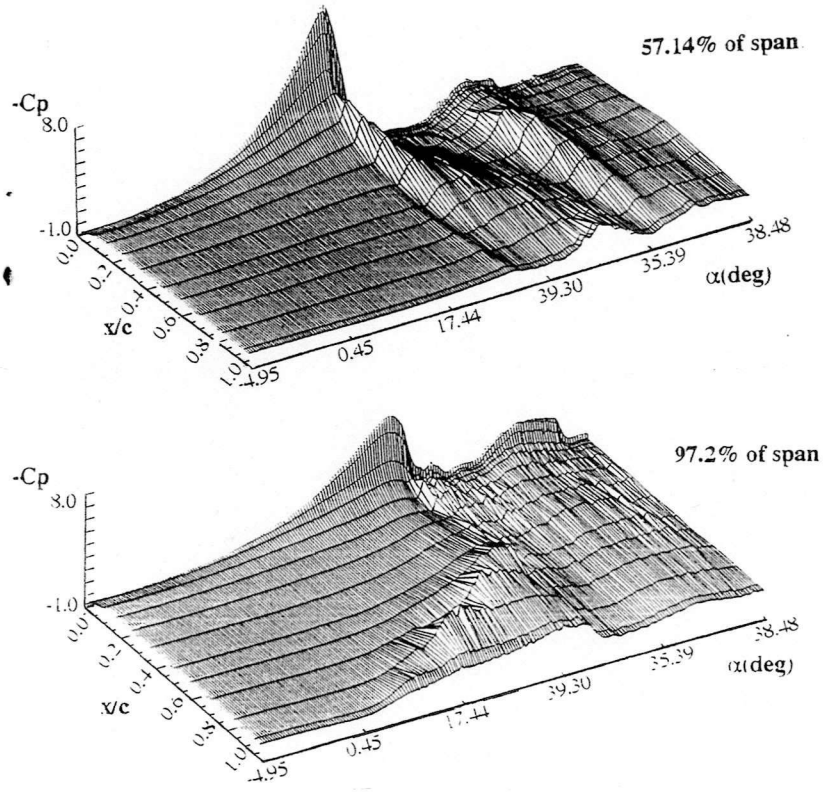

Fig. 4 Chordwise Cp against α at two spanwise sections

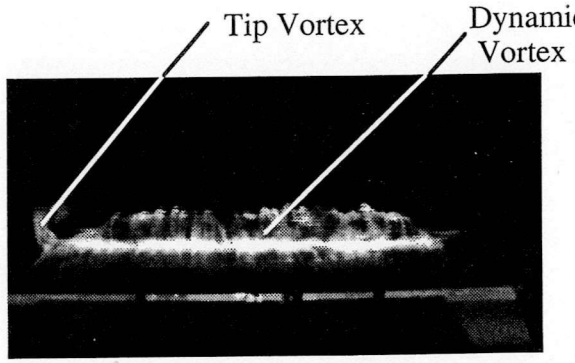

(a) Initial development of dynamic stall vortex

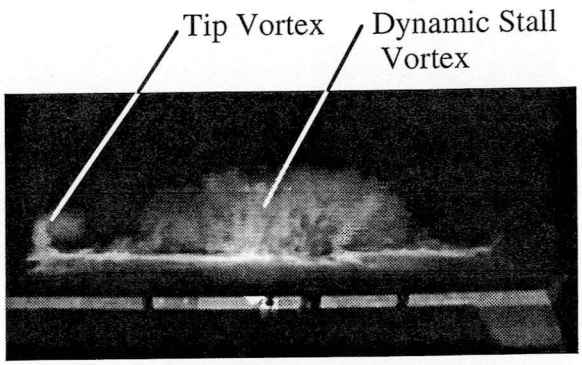

(b) Distortion of dynamic stall vortex

Fig. 5. Flow visualisation of the development of the dynamic stall vortex

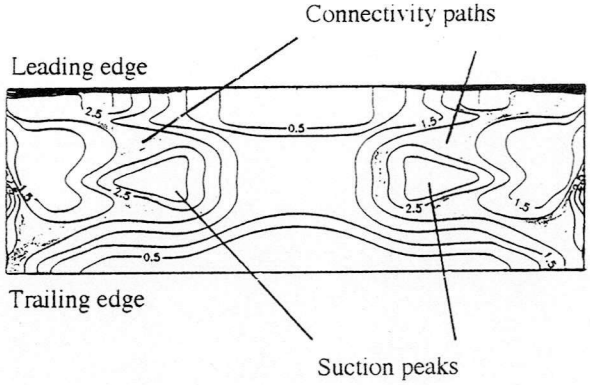

Fig. 6. Surface Cp contours at end of ramp motion